High-spin states in ^{109}Te: Competition between collective and single-particle excitations

A. J. Boston,[1] E. S. Paul,[1,*] C. J. Chiara,[2] M. Devlin,[3,†] D. B. Fossan,[2] S. J. Freeman,[4] D. R. LaFosse,[3,‡] G. J. Lane,[2,§] M. Leddy,[4] I. Y. Lee,[5] A. O. Macchiavelli,[5] P. J. Nolan,[1] D. G. Sarantites,[3] J. M. Sears,[2] A. T. Semple,[1] J. F. Smith,[2,‖] and K. Starosta[2]

[1]*Oliver Lodge Laboratory, University of Liverpool, P.O. Box 147, Liverpool L69 7ZE, United Kingdom*

[2]*Department of Physics and Astronomy, State University of New York at Stony Brook, Stony Brook, New York 11794*

[3]*Department of Chemistry, Washington University, St. Louis, Missouri 63130*

[4]*Schuster Laboratory, University of Manchester, Brunswick Street, Manchester M13 9PL, United Kingdom*

[5]*Nuclear Science Division, Lawrence Berkeley National Laboratory, Berkeley, California 94720*

(Received 10 January 2000; published 10 May 2000)

High-spin states have been studied in neutron-deficient $^{109}_{52}$Te, populated through the ^{58}Ni(^{58}Ni, $\alpha 2pn$) reaction at 250 MeV. The GAMMASPHERE γ-ray spectrometer has been used in conjunction with the MICROBALL charged-particle detector and 15 neutron detectors in order to select weakly populated evaporation residues. New band structures have been established in ^{109}Te. Measured $B(E1)$ strengths are discussed in terms of octupole correlations in this mass region. In addition, possible noncollective oblate states have been identified.

PACS number(s): 27.60.+j, 23.20.Lv, 21.10.Re

I. INTRODUCTION

A variety of exotic nuclear structure effects is encountered in neutron-deficient nuclei close to the $N = Z = 50$ shell closures. The limited number of valence particles outside the ^{100}Sn doubly magic core is insufficient to induce significant quadrupole deformation; hence these nuclei provide an ideal case in which to observe competition between collective and single-particle degrees of freedom. For example, specific noncollective aligned states compete with weakly deformed collective structures at relatively low spin in the tellurium ($Z=52$) isotopes [1]. In addition, the observation of enhanced $E1$ strength suggests that octupole correlations are important in this mass region [2–6].

This paper presents new results for odd-N ^{109}Te, obtained using the GAMMASPHERE spectrometer augmented by ancillary charged-particle and neutron detectors. Excited states were first identified in this nucleus following γ-ray correlation with β-delayed protons and alpha particles using the recoil decay tagging (RDT) technique at Daresbury Laboratory [7]. A parallel study established states in ^{109}Te directly by in-beam spectroscopy using the NORDBALL array in conjunction with charged-particle and neutron detectors [8]. A recent study of ^{109}Te, using the GASP array with charged-particle detectors, has discussed rotationally induced octupole collectivity at high spin [5].

*Corresponding author. Electronic address: esp@ns.ph.liv.ac.uk

†Present address: LANSCE-3, Los Alamos National Laboratory, Los Alamos, NM 87545.

‡Present address: Department of Physics and Astronomy, State University of New York at Stony Brook, Stony Brook, NY 11794.

§Present address: Nuclear Science Division, Lawrence Berkeley National Laboratory, Berkeley, CA 94720.

‖Present address: Schuster Laboratory, University of Manchester, Brunswick Street, Manchester M13 9PL, UK.

II. EXPERIMENTAL DETAILS

High-spin states in $A\sim 110$ nuclei were populated with the ^{58}Ni(^{58}Ni, $x\alpha\ yp\ zn\ \gamma$) fusion-evaporation reaction. In particular, states in the neutron-deficient ^{109}Te nucleus were populated through the $\alpha 2pn$ ($x=1$, $y=2$, $z=1$) exit channel. The experiment was performed at the Lawrence Berkeley National Laboratory, using a 250 MeV ^{58}Ni beam supplied by the 88-Inch Cyclotron. The beam was incident on two thin self-supporting nickel targets, each of nominal thickness 500 μg/cm^2 and enriched to $>97\%$ with ^{58}Ni. The GAMMASPHERE [9] γ-ray spectrometer, containing 83 HPGe detectors, was used in conjunction with the MICROBALL [10] charged-particle detector and an array of neutron detectors in order to provide clean exit channel selection through determination of the number of evaporated particles (x, y, z).

Coincident escape-suppressed γ-ray events were recorded to tape for events containing a minimum of three γ rays detected in prompt coincidence with a charged particle detected in the MICROBALL, i.e., $x+y>0$. The associated information from the neutron detectors was also recorded for off-line analysis. In 4 days of beam time, 1.4×10^9 such events were recorded.

An energy and efficiency calibration for the GAMMASPHERE array was achieved using standard ^{152}Eu, ^{60}Co, and ^{182}Ta sealed radioactive sources which were mounted at the target position. The data acquired from these sources enabled a good knowledge of the response of the spectrometer to be found for the broad range of γ-ray energies corresponding to those observed in this work.

A. Charged-particle and neutron detection

The MICROBALL [10] charged-particle detector was used to determine the number of evaporated alpha particles (x) and protons (y) associated with an event. The MICROBALL consists of 95 closely packed Cs(Tl) scintillators covering 97% of 4π. A combination of pulse-shape dis-

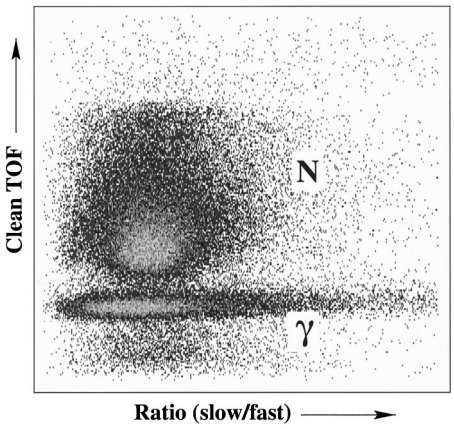

FIG. 1. Two-dimensional plot showing the neutron-γ discrimination achieved for one of the neutron detectors. The *y* axis is related to ''time-of-flight'' information, while the *x* axis is related to ''pulse-shape-discrimination'' information, namely, a ratio of the slow and fast components of the scintillator signal.

crimination (PSD) and zero-crossover timing (ZCT) can be used to separate light charged particles, including protons and alpha particles, as detailed in Ref. [10].

Fifteen large-volume NE213 liquid-scintillator neutron detectors were mounted in the three most forward rings of the GAMMASPHERE frame, replacing the HPGe detectors in those rings. Ten of the detectors came from the U.K. and five from the University of Pennsylvania. The total efficiency for detection of a neutron was estimated as $\approx 5\%$. These detectors were used to determine the number of evaporated neutrons (*z*) associated with an event. Given the neutron-deficient nature of the compound system, ^{116}Ba* neutron evaporation is significantly reduced relative to charged-particle evaporation. The detection of a neutron, however, can be used to pick out weak exit channels. Since the neutron detectors are sensitive to γ rays, some form of neutron-γ discrimination is required. The neutron detectors were mounted 40 cm from the target position enabling time-of-flight (TOF) neutron-γ discrimination. In addition, pulse-shape discrimination was also used to separate neutrons and γ rays. An example of a two-dimensional (2D) plot showing the neutron-γ separation, achieved using a combination of these techniques, is shown in Fig. 1.

B. Kinematic Doppler correction

In order to populate neutron-deficient nuclei, such as ^{109}Te, the use of a symmetric reaction is required. Such an approach, combined with the use of a thin target, results in the residual nuclei having a large recoil velocity ($\sim 4.5\%\ c$). The observed γ rays therefore exhibit a Doppler shift in their measured energies. The Doppler correction has been achieved by knowing the recoil velocity v and the angle θ of each detector. The use of segmented detector technology in the GAMMASPHERE array allows the effective opening angle of the HPGe detectors to be reduced, further improving the observed γ-ray energy resolution.

The assumption that the recoils are emitted along the beam direction, while valid for fusion-evaporation reactions which result in heavy ($A \geqslant 120$) recoiling nuclei, becomes less valid for lighter systems. The emission of light particles, particularly α particles, has the effect of broadening the recoil cone and results in γ rays with a poor energy resolution (Doppler broadening) being observed. The quality of the γ-ray spectra studied in this work has greatly benefited from a kinematic Doppler reconstruction [10,11] performed using the MICROBALL. This approach typically yielded an improvement of 30% in the energy resolution of γ-ray transitions for the ^{109}Te exit channel.

C. Fold and sum-energy selection

In order to improve the channel selection further, the BGO anti-Compton shield elements of the GAMMASPHERE spectrometer were used as a γ-ray fold and sum-energy selection device. By removing the Hevimet collimators from the front of the HPGe detectors, the front of the BGO suppression shields were exposed, allowing γ rays to strike the shield elements directly. The number of BGO elements firing and their total recorded energy were recorded for each event providing fold (k) and sum-energy (H) information. By setting off-line software gates on a two-dimensional k-H plot, a significant improvement in the quality of the channel selection was made. Specifically, low k and H values enhanced the four-particle ^{109}Te channel.

III. RESULTS

A. Level scheme construction

The initial 1.4×10^9 events were reduced to 4.7×10^5 events following the selection of the ^{109}Te exit channel. The

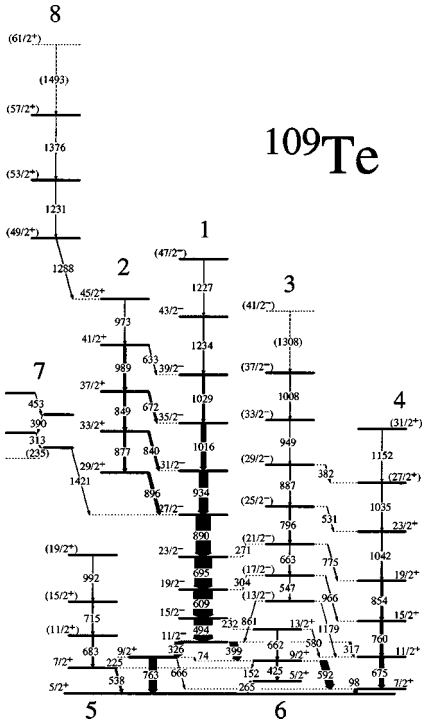

FIG. 2. Level scheme deduced for ^{109}Te from this work. The transition energies are given in keV and their relative intensities are proportional to the widths of the arrows. The $5/2^+$ ground-state assignment is taken from systematics.

TABLE I. Measured properties of the γ-ray transitions assigned to ^{109}Te.

E_γ (keV) [a]	I_γ [b]	A_2/A_0	A_4/A_0	δ	R [c]	Mult.	Assignment	Band
74	<1						$9/2^+ \rightarrow 9/2^+$	5→6
98.4	8.1	−0.250(75)	−0.001(93)	0.03(6)	0.90(10)	$M1/E2$	$7/2^+ \rightarrow 5/2^+$	4→5
152.5	<1						$9/2^+ \rightarrow 7/2^+$	6
225.3	13.1				0.75(4)	$M1/E2$	$9/2^+ \rightarrow 7/2^+$	5
232	<1						$15/2^- \rightarrow 13/2^+$	1→6
234.9	<1							8
265.5	11.0				0.71(6)	$M1/E2$	$5/2^+ \rightarrow 5/2^+$	6→5
271.0	<1						$(21/2^-) \rightarrow 23/2^-$	3→1
304	<1						$(17/2^-) \rightarrow 19/2^-$	3→1
312.9	<1							8
317.2	16.8	0.33(11)	≡0.0	−0.12(23)	1.02(8)	$E1$ [e]	$11/2^- \rightarrow 11/2^+$	1→4
326.5	56.7	−0.212(26)	−0.046(33)	0.033(39)	0.61(3)	$E1$ [e]	$11/2^- \rightarrow 9/2^+$	1→5
382	<1						$(29/2^- \rightarrow 27/2^+)$	3→4
389.9	<1							8
399.2	61.0	−0.226(30)	0.010(37)	0.025(25)	0.64(3)	$E1$ [e]	$11/2^- \rightarrow 9/2^+$	1→3
424.8	9.8	0.17(12)	−0.02(15)		0.97(5)	$E2$	$9/2^+ \rightarrow 5/2^+$	6
452.5	<1							8
494.5	≡100	0.283(21)	0.003(26)		1.10(4)	$E2$	$15/2^- \rightarrow 11/2^-$	1
530.7	<1						$(25/2^-) \rightarrow 23/2^+$	3→4
538.5	10.7	−0.45(13)	≡0.0	−0.086(83)	0.80(6)	$M1/E2$	$7/2^+ \rightarrow 5/2^+$	5
547.0	<1						$(17/2^- \rightarrow 13/2^-)$	3
580.0	<1						$13/2^+ \rightarrow 11/2^+$	6→4
592.1	33.5	−0.103(37)	≡0.0	0.102(23)	0.69(3)	$M1/E2$	$9/2^+ \rightarrow 7/2^+$	6→4
609.1	89.5	0.331(21)	0.108(25)		1.02(3)	$E2$	$19/2^- \rightarrow 15/2^-$	1
632.6	3.3				0.58(8)	$E1$ [e]	$41/2^+ \rightarrow 39/2^-$	2→1
661.3	4.4				0.98(8)	$E2$	$13/2^+ \rightarrow 9/2^+$	6
663.3	7.2				1.03(7)	$E2$	$(21/2^- \rightarrow 17/2^-)$	3
665.8	<1						$9/2^+ \rightarrow 7/2^+$	5→4
672.2	4.4				0.88(7) [d]	$E1$ [e]	$37/2^+ \rightarrow 35/2^-$	2→1
674.5	27.0				0.88(7) [d]	$E2$	$11/2^+ \rightarrow 7/2^+$	4
682.9	8.2						$(11/2^+) \rightarrow 7/2^+$	5
695.2	80.1	0.330(22)	0.009(27)		1.00(3)	$E2$	$23/2^- \rightarrow 19/2^-$	1
715.1	6.7						$(15/2^+ \rightarrow 11/2^+)$	5
760.3	8.3	0.277(41)[d]	≡0.0		0.88(3) [d]	$E2$	$15/2^+ \rightarrow 11/2^+$	4
763.2	43.7	0.277(41)[d]	≡0.0		0.88(3) [d]	$E2$	$9/2^+ \rightarrow 5/2^+$	5
775.3	2.7						$(21/2^-) \rightarrow 19/2^+$	3→4
796.2	5.2						$(25/2^- \rightarrow 21/2^-)$	3
839.6	8.6	−0.42(16)	0.17(20)	−0.11(12)	0.80(7)	$E1$ [e]	$33/2^+ \rightarrow 31/2^-$	2→1
848.8	20.2				0.90(7) [d]	$E2$	$37/2^+ \rightarrow 33/2^+$	2
853.8	20.2				0.90(7) [d]	$E2$	$19/2^+ \rightarrow 15/2^+$	4
861.0	<1						$(13/2^-) \rightarrow 11/2^-$	3→1
877.4	14.5	0.259(81)	0.107(99)		0.89(6)	$E2$	$33/2^+ \rightarrow 29/2^+$	2
886.7	3.0						$(29/2^- \rightarrow 25/2^-)$	3
889.6	62.7	0.379(27)	≡0.0		1.01(5)	$E2$	$27/2^- \rightarrow 23/2^-$	1
895.7	14.7	−0.308(73)	≡0.0	−0.04(15)	0.62(8)	$E1$ [e]	$29/2^+ \rightarrow 27/2^-$	2→1
933.7	34.3	0.348(41)	0.087(49)		1.01(4)	$E2$	$31/2^- \rightarrow 27/2^-$	1
949.0	<1						$33/2^- \rightarrow 29/2^-$	3
957	<1						$\rightarrow 47/2^-$	→1
966.0	<1						$(17/2^-) \rightarrow 15/2^+$	3→4
973.4	9.3	0.51(12)	≡0.0		0.93(6)	$E2$	$45/2^+ \rightarrow 41/2^+$	2
989.4	30.6	0.209(62)	≡0.0		0.93(6)	$E2$	$41/2^+ \rightarrow 37/2^+$	2
991.5	3.9						$(19/2^+ \rightarrow 15/2^+)$	5

TABLE I. (*Continued*).

E_γ (keV) [a]	I_γ [b]	A_2/A_0	A_4/A_0	δ	R [c]	Mult.	Assignment	Band
1008.1	<1						$(37/2^-\rightarrow 33/2^-)$	3
1015.8	18.0	0.178(48)	−0.084(59)		0.96(5)	$E2$	$35/2^-\rightarrow 31/2^-$	1
1029.2	7.8				1.19(13)	$E2$	$39/2^-\rightarrow 35/2^-$	1
1035.3	4.9						$(27/2^+)\rightarrow 23/2^+$	4
1042.1	10.1				0.98(6)	$E2$	$23/2^+\rightarrow 19/2^+$	4
1048	<1						$(49/2^+\rightarrow 45/2^+)$	2
1151.6	1.1						$(31/2^+\rightarrow 27/2^+)$	4
1179	<1						$(13/2^-)\rightarrow 11/2^+$	3→4
1227	7.5[d]				1.20(9) [d]	$E2$	$47/2^-\rightarrow 43/2^-$	1
1231	7.5[d]				1.20(9) [d]	$E2$	$(53/2^+\rightarrow 49/2^+)$	8
1234	7.5[d]				1.20(9) [d]	$E2$	$43/2^-\rightarrow 39/2^-$	1
1287.9	<1						$(49/2^+)\rightarrow 45/2^+)$	8→2
1308	<1						$(41/2^-\rightarrow 37/2^-)$	3
1376	<1						$(57/2^+\rightarrow 53/2^+)$	8
1421.0	1.7						$\rightarrow 27/2^-$	7→1
1493	<1						$(61/2^+\rightarrow 57/2^+)$	8

[a]The γ-ray energies are estimated to be accurate to ± 0.3 keV for the strong transitions ($I_\gamma > 10$), rising to ± 0.6 keV for the weaker transitions. Energies quoted as integers have errors ± 1 keV.

[b]Errors in the relative intensities are estimated to be less than 5% of the quoted values for strong transitions ($I_\gamma > 10$) and less than 10% for the weaker transitions.

[c]These ratios were obtained from a sum of gates on the 494 and 609 keV quadrupole transitions.

[d]Value given for the composite peak.

[e]The electric nature of this dipole transition is tentative.

data were then unfolded into constituent double (γ^2) coincidence events and replayed into a RADWARE [12] format matrix containing 2.2×10^6 γ-γ events. The data set was also unfolded into constituent triple (γ^3) coincidence events and replayed into a RADWARE [12] format cube containing 2.2×10^5 γ-γ-γ events. This may appear to be a very low amount of data to justify the construction of the cube; however, the data were of sufficient cleanliness that the cube greatly facilitated the analysis.

Analysis of the matrix was conducted using the ESCL8R graphical analysis package [12], while analysis of the cube was conducted using LEVIT8R [12]. The deduced level scheme of ^{109}Te is shown in Fig. 2, where the ordering of transitions is based on relative γ-ray intensities and triples (γ^3) coincidence relationships. The measured transition energies and the relative intensities of the ^{109}Te γ rays are listed in Table I. Examples of γ-ray spectra are presented in Fig. 3. Despite the gating conditions made to enhance the ^{109}Te ($\alpha 2pn$) channel, some contamination from ^{112}I ($3pn$) is evident in Fig. 3(a). This corresponds to the misidentification of a proton as an alpha particle and is related to the degradation of proton-alpha discrimination for low-energy charged particles detected in the most backward rings of the MICROBALL. The ^{109}Te transitions in Fig. 3(a) are, however, much stronger than the ^{112}I transitions, despite the fact that ^{112}I was populated with at least 15 times the strength of ^{109}Te in this reaction.

B. Spin and parity assignments

In order to establish transition multipolarities, an angular distribution analysis of the data was performed. After selecting transitions in ^{109}Te with the ancillary detectors, the γ-ray data were projected out into the rings of GAMMASPHERE at a given angle θ to the beam direction; 14 of the usual 17 rings were available, the three most forward rings containing the neutron detectors.

The transition intensities were determined in each ring and normalized using the total number of counts recorded in that ring. This rather simple approach however yielded reasonable results (see Fig. 4). The normalized intensities were then fitted to the angular distribution function

$$W(\theta)=A_0[1+(A_2/A_0)P_2(\cos\theta)+(A_4/A_0)P_4(\cos\theta)] \quad (1)$$

in order to extract the A_2/A_0 and A_4/A_0 coefficients; the results are included in Table I. For some of the weaker transitions or those with an unphysically large fitted A_4/A_0 value, A_4 was set to zero and only a value for A_2/A_0 extracted. Examples of the fitted angular distributions are shown in Fig. 4.

The angular distribution coefficients obtained for the dipole transitions were used to extract multipole mixing ratios following the formalism of Ref. [13] and also using the phase convention of Ref. [13]. These results are also included in Table I. Apart from the 592 keV ($9/2^+\rightarrow 7/2^+$) transition linking bands 4 and 6, and perhaps the 538 keV ($7/2^+\rightarrow 5/2^+$) transition of band 5, the multipole mixing ratios are all consistent with zero. Hence the majority of the dipole transitions are assigned here as $E1$ transitions since $M2$ admixture would be negligible. Although the GAMMASPHERE segmented HPGe detectors offer some degree of

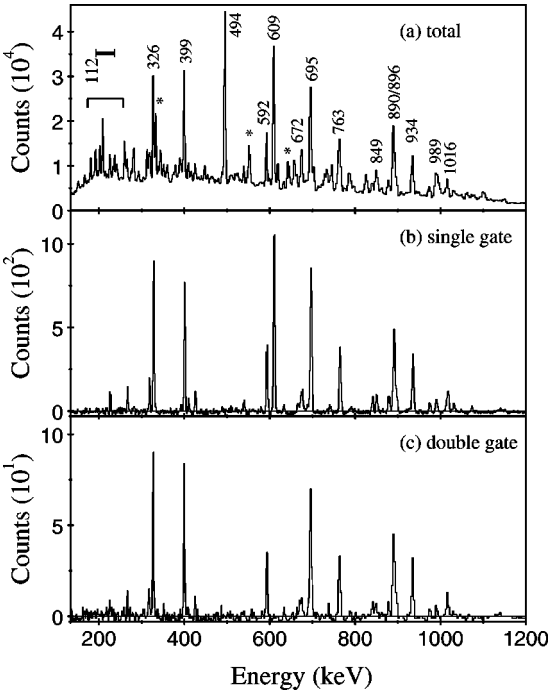

FIG. 3. Examples of γ-ray spectra showing transitions in ^{109}Te. A total projection of the $\alpha 2pn$-gated γ-γ matrix is shown in (a) with transition energies labeled in keV. The low-energy transitions around 200 keV, together with the transitions labeled by the asterisks, are contamination from ^{112}I, as discussed in the text. A background-subtracted gate on the 494 keV transition, obtained from the γ-γ matrix, is shown in (b), while a background-subtracted double gate on the 494 and 609 keV transitions, obtained from the γ-γ-γ cube, is shown in (c).

sensitivity to γ-ray polarizations [14], i.e., electric or magnetic character, our experience shows that meaningful results can only be obtained for very strong transitions [16] in accordance with the conclusions of Ref. [14]. The ^{109}Te transitions are too weak for such an analysis.

An average angular intensity ratio, defined as

$$R=\frac{I_{\gamma\gamma}(\theta_1\approx 50°,130°,\theta_2=\text{all})}{I_{\gamma\gamma}(\theta_1\approx 90°,\theta_2=\text{all})}, \tag{2}$$

was also evaluated for the transitions. Here the coincident intensities $I_{\gamma\gamma}$ were measured at an angle θ_1 when gated by quadrupole transitions at an angle θ_2. This approach yields theoretical R values for pure stretched quadrupole and pure stretched dipole transitions of approximately 1.00 and 0.63, respectively. These results are also included in Table I.

C. Band structures in ^{109}Te

The strongly populated band 1 (Fig. 2) has been previously discussed in Refs. [7,8,5], where it has been associated with the favored signature component of a negative-parity $\nu h_{11/2}$ intruder orbital. Band 2, a high-spin positive-parity band, has also been observed previously [5], although it was

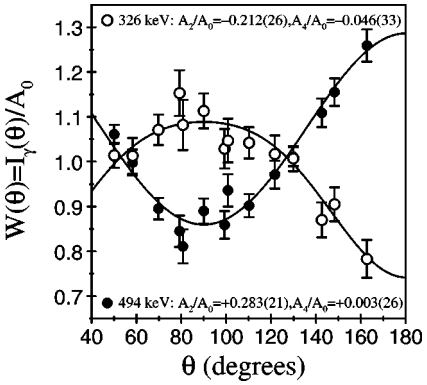

FIG. 4. Examples of angular distributions for quadrupole (494 keV) and dipole (326 keV) transitions. Experimental intensities are shown by the data points, while fitted angular distribution functions are shown by the curves.

assigned negative parity in Ref. [8]. The present angular distribution results are consistent with pure stretched dipole assignments for the linking transitions between bands 2 and 1, which are hence assigned $E1$ transitions in agreement with Ref. [5]. Band 1 is in agreement with Ref. [5] only up to the $43/2^-$ level. The higher transitions have been been placed in a separate band (band 8) that feeds band 2, rather than band 1. The placement of the transitions is hampered by the observation of a triplet of γ rays with energies $\approx$1231 keV. A 1227 keV transition is placed in band 1 above the known 1234 keV transition, while a 1231 keV transition is placed in band 8. The improved energy resolution at this energy, $\Delta E_\gamma \approx 6.0$ keV, afforded by the kinematic Doppler correction greatly helped in the establishment of the three γ rays of similar energy.

The $11/2^-$ bandhead of band 1 decays to low-spin positive-parity states associated with $\nu g_{7/2}$ and $\nu d_{5/2}$ orbitals. Two strong depopulating transitions of stretched dipole ($E1$) character (326 keV and 399 keV) feed $9/2^+$ states of bands 5 and 6, respectively. The 763 keV quadrupole transition depopulating the $9/2^+$ state of band 5 is assumed to feed the $5/2^+$ ground state of ^{109}Te. Previous work has assigned the ground state as $5/2^+$ through comparison with interacting boson-fermion model (IBFM) calculations [8]; this is also consistent with systematics of light odd-N tellurium isotopes. The ground state is associated with predominantly $\nu d_{5/2}$ character.

Band 3 is newly identified, as is band 4 above the $19/2^+$ state [8] and band 5. Band 4 may be associated with the favored signature of a $\nu g_{7/2}$ orbital [8], while the short band 6 represents the unfavored component. Similarly, band 5 can be associated with a $\nu d_{5/2}$ orbital. Band 3 feeds both bands 1 and 4. The position of the energy levels of band 3 with respect to band 1 suggests that it is the signature partner of band 1, built on the unfavored component of the $\nu h_{11/2}$ orbital. A large signature splitting ($\sim$500 keV) is consistent with the decoupled nature ($\Omega=1/2$) of the $\nu h_{11/2}$ orbital. These arguments lead to the tentative spin and parity assignments of band 3 shown in Fig. 2.

A weakly populated structure (band 7) feeds band 1 at $27/2^-$ through a high-energy 1421 keV transition of undeter-

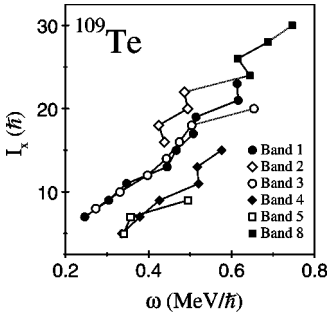

FIG. 5. Total aligned angular momentum I_x of the bands in ^{109}Te plotted as a function of rotational frequency.

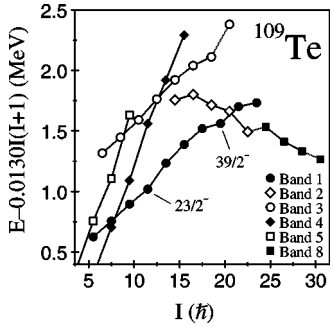

FIG. 6. Experimental rigid-rotor plot for the bands in ^{109}Te. The favored states labeled by their spins and parities may correspond to aligned noncollective oblate states; configurations are given in the text.

mined multipolarity. The low energy of the transitions within band 7, together with their regular increase in energy, suggests a $\Delta I=1$ structure of magnetic dipole transitions.

IV. DISCUSSION

In common with other tellurium isotopes, ^{109}Te is expected to possess a small quadrupole ground-state deformation [$\varepsilon_2 \sim 0.135$ from total Routhian surface (TRS) calculations] and hence a low-spin decay scheme dominated by single-particle effects. The complicated pattern of positive-parity, irregularly spaced γ-ray transitions observed below the $11/2^-$ state in ^{109}Te has been interpreted in terms of quasineutron excitations involving the $d_{5/2}$ and $g_{7/2}$ orbitals coupled to quadrupole vibrations [8]. Calculations in the vibrational limit of the IBFM have been discussed in Ref. [8]. The total aligned angular momenta $I_x=\sqrt{I(I+1)-K^2}$ of the bands in ^{109}Te are shown in Fig. 5 as a function of rotational frequency. Bands 1 and 3 show values of I_x consistent with a nonrotational interpretation. This allows these structures to be explained in terms of the $\nu h_{11/2}$ orbital coupled to the yrast states in the underlying even-even ^{108}Te core [4]. Bands 4 and 5 may be similarly interpreted as $\nu g_{7/2}$ and $\nu d_{5/2}$ orbitals, respectively, coupled to the yrast states of the core.

A. Aligned noncollective oblate states

^{109}Te manifests several unexpectedly low-lying (energetically favored) states similar to those observed in other light tellurium nuclei [1]. These can be seen in Fig. 6, which shows the energy levels minus a rigid-rotor reference, as a function of spin. Inspection of this figure reveals $23/2^-$, $39/2^-$ low-lying states, which are labeled for clarity. These states could correspond to noncollective oblate configurations, where a subset of the valence nucleons generate the entire nuclear spin by aligning their single-particle angular momenta. Alternatively, the experimental states could just represent core-particle coupled states that are perturbed by the presence of the energetically competing noncollective states. In the following discussion, we propose single-particle configurations for these noncollective states.

The $23/2^-$ state is seen to be particularly favored in Fig. 6. A noncollective state at this spin can be generated by the fully aligned $\{\pi[(g_{7/2}/d_{5/2})^2_{6^+}]\otimes\nu[(h_{11/2})_{11/2^-}]\}_{23/2^-}$ configuration. The $39/2^-$ state is another particularly low-lying point on the rigid-rotor plot. It may present evidence for an aligned noncollective state based on the $\{\pi[(g_{7/2}/d_{5/2})^2_{6^+}]\otimes\nu[(h_{11/2})^3_{27/2^-}]\}_{39/2^-}$ configuration. Similar low-lying $23/2^-$ and $39/2^-$ states have been experimentally observed in a number of heavier odd tellurium isotopes [1].

B. Particle-hole excitations

Band 7 offers evidence for a one-particle–one-hole excitation across the $Z=50$ shell gap. Such excitations, involving a single high-Ω $\pi g_{9/2}$ hole, produce $\Delta I=1$ structures in this mass region.

It can be seen in Fig. 6 that band 8 is yrast above 45/2 and that the energies of its levels decrease, with increasing spin, relative to the rigid-rotor reference. Such behavior is characteristic of a smooth terminating band [15] involving a two-particle–two-hole excitation across the $Z=50$ shell gap (e.g.,

TABLE II. Measured electric dipole strengths in ^{109}Te, extracted for the tentative $E1$ transitions, assuming $Q_0=200\ e\ \mathrm{fm}^2$.

E_γ (keV)	$I_i^\pi\rightarrow I_f^\pi$	Band	$B(E1)/B(E2)$ (10^{-6} fm^{-2})	$B(E1)$ ($10^{-3}\ e^2$ fm^2)	$B(E1)$ 10^{-3} (W.u.)	$\lvert D_0\rvert$ (e fm)
633	$41/2^+\rightarrow 39/2^-$	$2\rightarrow 1$	1.01(9)	1.42(10)	0.96(9)	0.111(10)
672	$37/2^+\rightarrow 35/2^-$	$2\rightarrow 1$	1.09(8)	1.52(10)	1.03(8)	0.115(10)
840	$33/2^+\rightarrow 31/2^-$	$2\rightarrow 1$	1.02(7)	1.40(8)	0.95(6)	0.110(8)
775	$21/2^-\rightarrow 19/2^+$	$3\rightarrow 4$	0.08(4)	0.11(5)	0.08(4)	0.031(15)
966	$17/2^-\rightarrow 15/2^+$	$3\rightarrow 4$	0.05(3)	0.06(3)	0.04(2)	0.024(12)

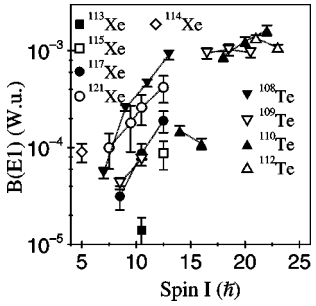

FIG. 7. Experimental $B(E1;I\rightarrow I-1)$ strengths in ^{109}Te and neighboring nuclei, taken from Ref. [6]. Results for the $E1$ transitions linking bands 2 and 1 (high spin), and bands 3 and 4 (low spin), in ^{109}Te are included.

$\pi h_{11/2}^2 g_{9/2}^{-2}$). The decay properties of band 8 are also remarkably similar to the strongest terminating band in neighboring ^{110}Te [16]. This latter band also decays into a high-spin positive-parity structure that is linked to negative-parity yrast states through strong $E1$ transitions.

C. $B(E1)$ strengths and octupole collectivity

Band 2 has been assigned positive parity following the establishment of inferred electric dipole ($E1$) transitions linking this structure to band 1. A number of inferred electric dipole transitions are also observed to link band 3 to band 4. Confirmation of the electromagnetic nature of these dipole transitions, perhaps through a measurement of the linear polarization of the γ rays, is therefore paramount in order to firmly establish their character. However, for the following discussion, we assume stretched $E1$ character for these transitions.

The magnitude of the intrinsic electric dipole moment, D_0, for ^{109}Te has been extracted by measurement of γ-ray branching ratios, using the recipe described in Ref. [6]. The experimental $B(E1)$ values were computed using a quadrupole moment estimate of $Q_0=200\ e\ \mathrm{fm}^2$, obtained from TRS calculations. The results, including $B(E1)/B(E2)$ ratios of reduced transition probabilities, $B(E1)$ strengths, and estimated D_0 values, are summarized in Table II. The use of an assumed value of Q_0 means that the absolute values for $B(E1)$ and D_0 should only be considered accurate to $\pm 25\%$. The present values of $B(E1)/B(E2)\approx 10^{-6}\ \mathrm{fm}^{-2}$ are consistent with those reported in Ref. [5]. The magnitudes of the D_0 results obtained for the $E1$ transitions linking bands 2 and 1 are remarkably similar to the those deduced in ^{110}Te [3] and ^{112}Te [4] at high spin ($I\gtrsim 15\hbar$). A similar analysis of the $E1$ transitions linking bands 3 and 4 yields a magnitude for D_0 which is four times smaller, although at lower spin ($I\lesssim 10\hbar$).

The observation of ''enhanced'' $E1$ strength in nuclei [usually taken as $B(E1)>10^{-5}$ Weisskopf units (W.u.)] is often cited as evidence for octupole correlations in nuclei. The systematics of $B(E1)$ strengths extracted in this mass region have been discussed in Ref. [6] as a function of spin, and are shown here in Fig. 7, while $B(E1)$ strengths for particular tellurium isotopes are given in Refs. [3–5,16]. The strongest $E1$ strengths are observed for the near-spherical tellurium isotopes at high spin, which appear to saturate at $B(E1)\sim 10^{-3}$ W.u. for ^{109,110,112}Te. These latter values are similar to those found in neutron-rich barium ($Z=56$) nuclei and are slightly smaller than values typical of the radium-thorium region (see, for example, Refs. [17,18] and references therein); both these mass regions offer strong evidence for octupole collectivity.

In the mass $A\sim 110$ region, octupole collectivity may be expected since both proton and neutron orbitals with $\Delta N=1$ and $\Delta j=\Delta l=3$ ($h_{11/2}$ and $d_{5/2}$) are near the Fermi surface. The strongest effects have been calculated for barium ($Z=56$), xenon ($Z=54$), and tellurium ($Z=52$) isotopes with $N\approx 56$ [19], albeit at low spin. Indeed, these nuclei are predicted to show a softness with respect to octupole deformation in their ground states. Calculations using Hartree-Fock+BCS (static correlations) and generator-coordinate (dynamical correlations) methods [20] suggest that octupole collectivity is enhanced by dynamical correlations. It is also possible that rotation could enhance octupole effects, and it has been suggested that nuclei with dynamical octupole deformations at low spin could develop static octupole deformation at high spin [21]. Furthermore, rotationally induced octupole collectivity has recently been discussed theoretically for ^{109}Te [5]. The enhanced $B(E1)$ strength between bands 2 and 1 in ^{109}Te suggests that band 2 may be interpreted as the coupling of an octupole phonon to the band 1 configuration.

V. CONCLUSIONS

By using ancillary charged-particle and neutron detectors with the GAMMASPHERE array, it has been possible to cleanly select transitions in ^{109}Te and study high-spin states in this neutron-deficient nucleus. This nucleus appears to show competition between single-particle and weakly collective structures. Several favored noncollective states have been proposed. In addition, the observation of enhanced $E1$ strength, albeit at high spin, suggests that octupole correlations are important in this mass region. It must be emphasized, however, that the $E1$ character of the dipole transitions in this mass region is only inferred through angular intensity measurements. Further measurements, in particular γ-ray linear polarizations, are certainly warranted to confirm the electric nature of these dipole transitions and put the octupole correlation interpretation on a firmer footing.

ACKNOWLEDGMENTS

This work was supported in part by the U.S. National Science Foundation and the U.K. Engineering and Physical Sciences Research Council. We are indebted to Prof. D.P. Balamuth of the State University of Pennsylvania for providing five of the neutron detectors used in this work and to Dr. D.C. Radford for providing the RADWARE analysis codes.

[1] E.S. Paul, D.B. Fossan, J.M. Sears, and I. Thorslund, Phys. Rev. C **52**, 2984 (1995).
[2] S.L. Rugari *et al.*, Phys. Rev. C **48**, 2078 (1993).
[3] E.S. Paul, H.R. Andrews, V.P. Janzen, D.C. Radford, D. Ward, T.E. Drake, J. DeGraaf, and S. Pilotte, Phys. Rev. C **50**, R534 (1994).
[4] G.J. Lane *et al.*, Phys. Rev. C **57**, R1022 (1998).
[5] G. de Angelis *et al.*, Phys. Lett. B **437**, 236 (1998).
[6] E.S. Paul *et al.*, Nucl. Phys. **A644**, 3 (1998).
[7] E.S. Paul *et al.*, Phys. Rev. C **51**, 78 (1995).
[8] Zs. Dombradi *et al.*, Phys. Rev. C **51**, 2394 (1995).
[9] I.Y. Lee, Nucl. Phys. **A520**, 641c (1990).
[10] D.G. Sarantites, P.-F. Hua, M. Devlin, L.G. Sobotka, J. Elson, J.T. Hood, D.R. LaFosse, J.E. Sarantites, and M.R. Maier, Nucl. Instrum. Methods Phys. Res. A **381**, 418 (1996).
[11] D. Seweryniak, J. Nyberg, C. Fahlander, and A. Johnson, Nucl. Instrum. Methods Phys. Res. A **340**, 353 (1994).
[12] D.C. Radford, Nucl. Instrum. Methods Phys. Res. A **361**, 297 (1995); **361**, 306 (1995).
[13] T. Yamazaki, At. Data Nucl. Data Tables **3**, 1 (1967).
[14] G.J. Schmid *et al.*, Nucl. Instrum. Methods Phys. Res. A **417**, 95 (1998).
[15] I. Ragnarsson, V.P. Janzen, D.B. Fossan, N.C. Schmeing, and R. Wadsworth, Phys. Rev. Lett. **74**, 3935 (1995).
[16] A.J. Boston, Ph.D. thesis, University of Liverpool, 1999.
[17] P.A. Butler and W. Nazarewicz, Nucl. Phys. **A533**, 249 (1991).
[18] P.A. Butler and W. Nazarewicz, Rev. Mod. Phys. **68**, 349 (1996).
[19] J. Skalski, Phys. Lett. B **238**, 6 (1990).
[20] P.-H. Heenen, J. Skalski, P. Bonche, and H. Flocard, Phys. Rev. C **50**, 802 (1994).
[21] R.V. Jolos and P. von Brentano, Phys. Rev. C **49**, R2301 (1994).